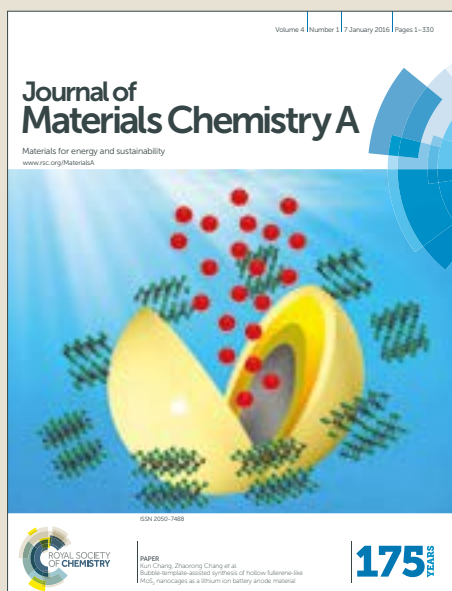


# Journal of Materials Chemistry A

Accepted Manuscript



This article can be cited before page numbers have been issued, to do this please use: G. M. Lari, A. Brucoli Leme de Moura, L. Weimann, S. Mitchell, C. Mondelli and J. Perez-Ramirez, *J. Mater. Chem. A*, 2017, DOI: 10.1039/C7TA02061A.



This is an Accepted Manuscript, which has been through the Royal Society of Chemistry peer review process and has been accepted for publication.

Accepted Manuscripts are published online shortly after acceptance, before technical editing, formatting and proof reading. Using this free service, authors can make their results available to the community, in citable form, before we publish the edited article. We will replace this Accepted Manuscript with the edited and formatted Advance Article as soon as it is available.

You can find more information about Accepted Manuscripts in the [author guidelines](#).

Please note that technical editing may introduce minor changes to the text and/or graphics, which may alter content. The journal's standard [Terms & Conditions](#) and the ethical guidelines, outlined in our [author and reviewer resource centre](#), still apply. In no event shall the Royal Society of Chemistry be held responsible for any errors or omissions in this Accepted Manuscript or any consequences arising from the use of any information it contains.



## ARTICLE

## Design of a technical Mg-Al mixed oxide catalyst for the continuous manufacture of glycerol carbonate

G. M. Lari, A. B. L. de Moura, L. Weimann, S. Mitchell, C. Mondelli\* and J. Pérez-Ramírez\*

Received 00th January 20xx,  
Accepted 00th January 20xx

DOI: 10.1039/x0xx00000x

[www.rsc.org/](http://www.rsc.org/)

The availability of a heterogeneous catalyst, which contains cheap and abundant elements, has a scalable synthesis, is highly active and stable, retains its performance upon shaping into a technical form and can be operated in continuous mode, would pave the way for a more ecological and economical production of glycerol carbonate from glycerol and urea. Here, we show that a mixed oxide of Mg and Al is a promising active phase for this reaction. The solid comprises widely available and non-toxic metals, is easily obtained through the thermal decomposition of a hydrotalcite-like material and can almost match the product yield of state-of-the-art Zn-based catalysts, while displaying an outstanding resistance against leaching, which causes the rapid dissolution of the latter. In-depth characterisation uncovered that Lewis-basic centres are crucial to activate glycerol through dehydrogenation. Their concentration was maximised by optimising the composition and calcination temperature of the precursor, thus reaching up to 60% glycerol carbonate yield. Millimeter-sized extrudates showing comparable basic properties to the powder sample, a well-developed meso- and macroporosity and high mechanical stability are obtained using a natural clay, bentonite, as a binder and thermally activating the hydrotalcite only after shaping. Upon testing in a continuous reactor under tuned conditions of temperature and pressure and in the presence of an aprotic solvent, the system shows the same glycerol yield as in the batch tests. During 100 h on stream, its activity decreases by 20% due to fouling, but can be fully restored upon burning-off of the carbonaceous deposits. This work discloses the development of a green material that exhibits high efficacy in a sustainable transformation, highlighting key parameters that should be generally taken into account in the design of an industrially-relevant chemocatalytic technology.

### Introduction

The interest in the valorisation of biomass and its more reactive nature compared to fossil-based feedstocks has propelled extensive research to design solid catalysts able to effectively convert bio-derived compounds into chemicals and fuels.<sup>[1]</sup> This endeavour does not only comprise the identification of a highly active and selective material. Indeed, various other criteria have to be fulfilled to ensure the viability, economical attractiveness and environmental friendliness of the overall process. The active phase should be composed of abundant, cheap and non-toxic chemical species and synthesised through scalable and non-energy intensive methods. Additionally, it should retain its performance upon formulation and shaping into a technical mm-sized body,

which can be handled in a safer and easier manner at a chemical plant and avoids pressure drops in fixed-bed reactors. While often seen as trivial, the frequent introduction of additives in appreciable amounts to facilitate the processing or enhance the properties of the resulting catalyst can lead to even drastic alterations of the structural, porous and chemical properties of the active phase. The interplay among components is typically emphasised under the conditions commonly experienced during preparation and use (elevated temperature and pressure, presence of water, *etc.*)<sup>[2]</sup> and its understanding is critical to optimise the catalytic behaviour. Last but not least, the solid should be robust and allow its utilisation in continuous-flow mode, which is industrially more relevant than batch operation owing to the greater scalability, safety and ease of control of the reaction conditions. Only a few works have reported about catalyst development addressing all or most of these aspects.<sup>[3]</sup> Recent examples comprise studies on Fe- and Sn-containing zeolites for the upgrading of glycerol, a widely available by-product of the biodiesel production, into the commodity chemical lactic acid.<sup>[4]</sup> Life cycle analysis indicated that using these chemocatalysts reduces the operating costs and ecological impact of the process compared to enzymatic alternatives, which are penalised by the typical high dilution of the feed

*Institute for Chemical and Bioengineering, Department of Chemistry and Applied Biosciences, ETH Zurich, Vladimir-Prelog-Weg 1, CH-8093 Zurich, Switzerland.*  
E-mails: cecilia.mondelli@chem.ethz.ch; jpr@chem.ethz.ch  
Electronic Supplementary Information (ESI) available: data on compositional, porous and basic properties of catalysts and binders, catalytic data of binders, photographs of the reaction mixtures after batch experiments, XRD and <sup>27</sup>Al MAS NMR spectroscopy of the rehydrated hydrotalcite, catalytic performance and pressure drop upon continuous operation of a non-shaped catalyst, EDX spectra of the fresh and used shaped catalysts and TGA of the sample in technical form after use for 100 h on stream. See DOI: 10.1039/x0xx00000x



**Scheme 1.** Modification of structural and basic properties of hydrotalcites upon thermal activation and subsequent rehydration.

stream and the consequent energy-demanding product separation.

Another relevant derivative of the triol, the preparation of which would benefit from a solid catalyst, is glycerol carbonate (4-(hydroxymethyl)-1,3-dioxolan-2-one, herein abbreviated as GC). This compound serves as a green solvent, humectant, agricultural additive and detergent<sup>[5]</sup> or as an intermediate for the preparation of monoglycerides, esters, polyglycerols and polyurethanes.<sup>[6]</sup> It is obtained reacting glycerol with a carbonating agent,<sup>[7]</sup> where urea is preferred in view of its condensed and harmless nature, the fast reaction rates and the easily separable (gaseous) secondary product generated.<sup>[8]</sup>

The reaction proceeds *via* the nucleophilic addition of two hydroxyl groups of the triol to urea, leading to the predominant formation of the 1,2-carbonate and the generation of two ammonia molecules.<sup>[9]</sup> It is industrially performed using salts of Zn, Mn, Mg, Fe, Cd and Ni, which contaminate the product stream in view of their homogeneous nature and thus impose high purification costs.<sup>[10]</sup> Additionally, most of these metals have a relatively high price and could represent a health hazard.

Aiming at identifying a greener alternative, the immobilisation of the cations onto an ion-exchange resin has been investigated<sup>[10b]</sup> but proof of their heterogeneous nature has not been provided.<sup>[11]</sup> Otherwise, various basic materials,<sup>[12]</sup> which enable the activation of alcoholic groups,<sup>[13]</sup> have been assessed. ZnO and Zn-containing mixed oxides stand as the most active catalysts (80–120 mmol<sub>GC</sub> h<sup>-1</sup> g<sub>cat</sub><sup>-1</sup>),<sup>[14]</sup> followed by MgO and CaO.<sup>[15]</sup> Hydrotalcite-like materials, also known as layered double hydroxides with the general formula  $[M^{2+}_n M^{3+}_m (\text{OH})_{2(n+m)}]^{m+} [A^{x-}]_{m/x} \cdot y\text{H}_2\text{O}$  and possessing low Brønsted-type basicity when  $M^{2+} = \text{Mg}^{2+}$  and  $M^{3+} = \text{Al}^{3+}$ ,  $A^{x-} = \text{CO}_3^{2-}$ , *i.e.*, the most common ions, exhibited a moderate activity.<sup>[16]</sup> Interestingly, rehydrated hydrotalcites, *i.e.*, materials obtained by replacing the  $\text{CO}_3^{2-}$  by  $\text{OH}^-$  through

thermal decomposition followed by hydration (**Scheme 1**), which feature stronger Brønsted basicity, and  $M^{2+}$ - $M^{3+}$  mixed oxides prepared by calcination of the hydrotalcite, which contain strong Lewis-basic sites, led to higher GC yields (up to 80% over the latter materials).<sup>[16a]</sup> Owing to their resistance to leaching, which contrasts the complete dissolution of Mg, Zn and Ca oxides, and the low price and toxicity of the metals contained, hydrotalcites and their derivatives appear most appealing for GC production. Still, these solids have only been evaluated in batch mode and their technical formulation has not been attempted.

Herein, shaped catalysts based on mixed oxides obtained from Mg–Al hydrotalcites are designed and demonstrated effective for the continuous preparation of GC from glycerol and urea. At first, since flow operation requires the use of a solvent, a suitable medium is identified *via* batch catalytic tests with ZnO. Then, various basic solids are screened, highlighting the superiority of hydrotalcite-derived Mg–Al mixed oxides for the target reaction also under diluted conditions. Thereafter, structure-properties relationships are established *via* in-depth characterisation and an optimised catalyst is attained by tuning synthesis and activation conditions. Then, a shaping protocol is developed to produce mm-sized extrudates possessing equivalent basic centres to the powder catalyst and adequate porosity, and their behaviour is evaluated in a prolonged run at suitable temperature and pressure. Finally, the predominant mechanism responsible for the moderate deactivation observed is identified and a strategy to restore the catalytic activity successfully applied.

## Experimental

### Catalyst preparation

Mg–Al hydrotalcites with a nominal Mg/Al ratio of 1, 2 or 4 were prepared by coprecipitation at a pH of 10. Briefly, 500 cm<sup>3</sup> of an aqueous solution of  $\text{Mg}(\text{NO}_3)_2 \cdot 6\text{H}_2\text{O}$  (0.25–1.00 M, Riedel-de Haen, >99%) and  $\text{Al}(\text{NO}_3)_3 \cdot 9\text{H}_2\text{O}$  (0.25 M, Sigma-Aldrich, >98%) were added to aqueous  $\text{Na}_2\text{CO}_3$  (2 M, 600 cm<sup>3</sup>, Sigma-Aldrich, >99.5%) at a rate of 3.5 cm<sup>3</sup> min<sup>-1</sup> while magnetically stirring (500 rpm) at 298 K. A concentrated (*ca.* 40 wt.%) NaOH solution was simultaneously added dropwise to keep the pH constant. The obtained slurry was aged at 333 K for 6 h under stirring. Then, the precipitate was filtered off, thoroughly washed with deionised water (*ca.* 100 cm<sup>3</sup> per gram of material) and dried at 338 K for 18 h. This solid was labelled as HTx, where x indicates the nominal Mg/Al ratio. A portion of the HTx samples was calcined in static air at 673–973 K for 6 h (5 K min<sup>-1</sup>) to obtain the corresponding Mg–Al mixed oxide (denoted as HTx-cy, where y designates the calcination temperature in K). In the case of HT2-c823, a part of the material was rehydrated by contact with decarbonated water for 1 h at 298 K under stirring (500 rpm). After the rehydration process, the sample was filtered off, washed with ethanol and dried in inert atmosphere. The thus obtained material was labelled as HT2-c823-r. Additional catalysts comprised  $\text{SiO}_2$  (Sipernat 120),  $\gamma\text{-Al}_2\text{O}_3$  (Sigma-Aldrich), ZnO

(Sigma-Aldrich, >97%), a Zn-Al mixed oxide (ZnHT-c823) obtained following the same protocol used for HT2-c823 but substituting the Mg precursor with Zn(NO<sub>3</sub>)<sub>2</sub>·6H<sub>2</sub>O (Sigma-Aldrich, 98%), a Zn-containing zeolite attained by three subsequent ion-exchange treatments of an MFI zeolite (nominal Si/Al = 40, Zeolyst International, CBV8014, code Z40) with a 0.1 M solution of Zn(NO<sub>3</sub>)<sub>2</sub>·6H<sub>2</sub>O (100 cm<sup>3</sup> per gram of zeolite each time), followed by calcination (823 K, 5 h, 5 K min<sup>-1</sup>) and an alkali-modified zeolite (Y-AT) prepared treating a zeolite Y (nominal Si/Al = 2.6, Zeochem) in a 0.1 M solution of H<sub>4</sub>-EDTA (373 K, 16 h, 100 cm<sup>3</sup> per gram of zeolite) and subsequently in a 0.3 M solution of NaOH (338 K, 0.5 h, 100 cm<sup>3</sup> per gram of zeolite), followed by calcination under the conditions mentioned above.<sup>[17]</sup>

### Catalyst forming

Catalysts in technical form were prepared by extrusion using kaolin (Sigma-Aldrich), bentonite (Sigma-Aldrich), montmorillonite (Sigma-Aldrich), SiO<sub>2</sub> (Sigma-Aldrich) or  $\gamma$ -Al<sub>2</sub>O<sub>3</sub> (Acros Organics, 99.9%) as the binder. HT2 (3.00 g) was homogenised with the binder (3.00 g) in the presence of ca. 6–10 g of water using a mechanical stirrer. The paste attained was extruded using a Mini-Screw Extruder (Caleva, 2 mm diameter) and the shaped bodies were calcined at 823 K for 5 h (5 K min<sup>-1</sup>) in static air. These catalysts were labelled as MgHT2-z-c823, where z is the first letter of the binder type.

### Catalyst characterisation

The metal content in the catalysts was determined by X-ray fluorescence spectroscopy (XRF) using an Orbis Micro XRF instrument equipped with a Rh source operated at 35 kV and 500  $\mu$ A. Powder X-ray diffraction (XRD) was performed using a PANalytical X'Pert PRO-MPD diffractometer with Ni-filtered Cu K $\alpha$  radiation ( $\lambda$  = 0.1541 nm), acquiring data in the 10–60° 2 $\theta$  range with an angular step size of 0.05° and a counting time of 2 s per step. N<sub>2</sub> sorption at 77 K was conducted using a Micromeritics TriStar analyser. Prior to the measurements, the solids were degassed at 573 K under vacuum for 3 h. Temperature-programmed desorption of carbon dioxide (CO<sub>2</sub>-TPD) was carried out using a Micromeritics Autochem II chemisorption analyser coupled with a MKS Cirrus 2 quadrupole mass spectrometer. For CO<sub>2</sub>-TPD, the catalyst (0.1 g) was pre-treated in a He flow (20 cm<sup>3</sup> min<sup>-1</sup>) at 373 K for 2 h. Afterwards, CO<sub>2</sub> (50 pulses, 1 cm<sup>3</sup>) diluted in He (10 cm<sup>3</sup> min<sup>-1</sup>) was adsorbed at 323 K, followed by He purging at the same temperature for 1 h. CO<sub>2</sub> desorption was performed using a He flow of 10 cm<sup>3</sup> min<sup>-1</sup> and monitored in the 323–973 K range (10 K min<sup>-1</sup>). The concentration of basic sites (C<sub>b</sub>) is expressed as  $\mu$ mol<sub>CO<sub>2</sub></sub> g<sup>-1</sup> and was obtained multiplying the area of the desorption curve by a calibration factor obtained from the decomposition of known amounts of Na<sub>2</sub>CO<sub>3</sub> (Sigma-Aldrich, >99.5%) and dividing it by the mass of the sample.<sup>27</sup> Al magic angle spinning nuclear magnetic resonance (MAS NMR) spectroscopy was conducted in a Bruker Avance 700 spectrometer operated at 182.4 MHz using 4-mm ZrO<sub>2</sub> rotors spun at 10 kHz. Spectra were acquired accumulating 512 scans using a pulse length of 1  $\mu$ s, a recycle

delay of 1 s, and solid (NH<sub>4</sub>)Al(SO<sub>4</sub>)<sub>2</sub> as a reference ( $\delta$  = 0.00 ppm). Thermogravimetric analysis (TGA) was performed in a Mettler Toledo TGA/DSC1 instrument equipped with a quadrupole mass spectrometer in the 298–1173 K range (10 K min<sup>-1</sup>) applying a N<sub>2</sub> flow of 60 cm<sup>3</sup> min<sup>-1</sup>. For the determination of coke residues on the used catalyst, 60 cm<sup>3</sup> min<sup>-1</sup> of air were used. Prior to the analysis, the samples were dried at 333 K for 2 h in a N<sub>2</sub> flow of 60 cm<sup>3</sup> min<sup>-1</sup>. Diffuse reflectance Fourier transform infrared (DRIFT) spectroscopy was conducted to study the decomposition of the hydrotalcite and the interaction of glycerol with KBr, HT2, HT2-c823 and HT2-c823-r using a Bruker Vertex 70 spectrometer equipped with a liquid-N<sub>2</sub> cooled MCT detector and a diffuse reflectance cell (Harrick). In the first type of experiment, the sample was degassed in Ar (10 cm<sup>3</sup> min<sup>-1</sup>) at 373 K for 4 h. Thereafter, the temperature was increased to 773 K (10 K min<sup>-1</sup>) and spectra were recorded every 50 K accumulating 64 scans in the 2300–1700 cm<sup>-1</sup> range with a resolution of 4 cm<sup>-1</sup>. For the second kind of measurements, spectra were recorded using the same settings as described above after contacting few milligrams of the liquid reactant with 100 mg of solid and degassing the obtained samples in Ar (10 cm<sup>3</sup> min<sup>-1</sup>) at 373 K for 1 h. Mercury porosimetry was carried out using a Micromeritics Autopore IV 9510 instrument (contact angle = 140°, pressure equilibration time = 10 s). The side crush strength of the extrudates was measured using a Dr. Schleuniger Pharmatron Tablet Tester 8M. Scanning electron (SEM) micrographs of internal cross-sections of the extrudates were acquired on a Quanta 200F instrument. Sample preparation involved embedding the extrudates in a resin (LR white medium grade) and trimming and cutting the embedded granules with a high-precision rotating disk covered with diamond powder (Leika TXP), resulting in a surface roughness of <1  $\mu$ m. Afterwards, the surfaces were polished by exposure to an argon ion beam (2 h, 4 kV, Hitachi IM4000). Finally, the samples were mounted on an aluminium holder and covered with a thin gold film (ca. 5 nm) to prevent charging. Scanning (STEM) and transmission (TEM) electron micrographs and elemental maps were acquired on a FEI Talos F200A instrument equipped with a high brightness field emission gun, a high-angle annular dark-field (HAADF) and a large collection angle energy-dispersive X-ray spectrometer (EDS) detector and operated at 200 kV. Beam transparent sections (80 nm thick) were obtained from the resin-embedded granules by ultramicrotomy, which were supported on copper grids coated with a continuous carbon film.

### Catalytic testing

Batch catalytic tests were carried out at 10 mbar in 50-cm<sup>3</sup> round bottomed flasks dipped in an oil bath heated at 373–473 K. For solvent-free experiments, the reactors were loaded with 0.06 mol of glycerol (Acros Organics, >99%) and urea (Sigma-Aldrich, >99.5%) and 1 g of catalyst. For measurements in the presence of a solvent, 0.006 mol of glycerol and urea, 0.1 g of catalyst and 9 g of solvent were introduced in the flasks. The reaction medium was water, methanol (Merck, 99.9%), ethanol (Sigma-Aldrich, 99.9%), 2-propanol (Sigma-

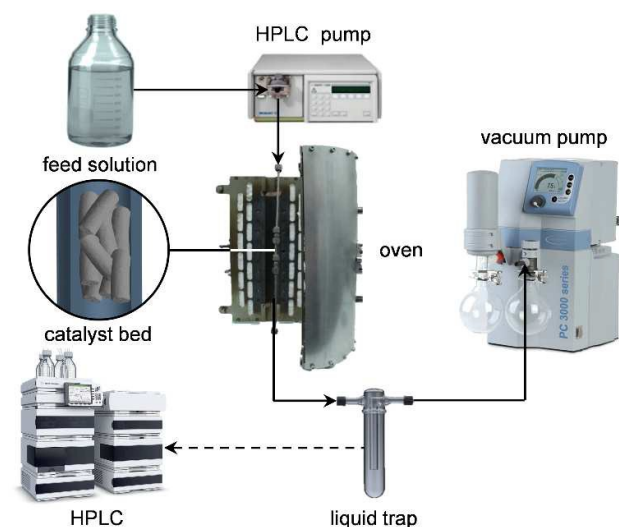


Figure 1. Scheme of the continuous-flow setup used in this study.

Aldrich, 99%), 1-butanol (Sigma-Aldrich, 99%), dimethyl formamide (Sigma-Aldrich, 99.9%), ethyl acetate (Sigma-Aldrich, >99.5%), dimethyl sulfoxide (Acros Organics, 99.9%),  $\gamma$ -butyrolactone (Sigma-Aldrich, >99%), acetone (Sigma-Aldrich, 99%) or acetonitrile (Sigma-Aldrich, 99.5%). The mixture was heated at the desired temperature under magnetic stirring (500 rpm) and allowed to react for 1 h. Then, the reaction was quenched using an ice bath and the catalyst removed using a Chromafil Xtra 0.25  $\mu\text{m}$  syringe filter.

Continuous-flow catalytic tests were performed using a homemade setup (Figure 1) comprising (i) a high-performance liquid chromatography (HPLC) pump (Gilson-306), (ii) a stainless steel tubular reactor with a precolumn (Swagelok SS-T4-S-035, o.d. =  $\frac{1}{4}$  inch, i.d. = 4.6 mm), both heated in a tubular oven, (iii) a gas-liquid separator and (iv) a vacuum pump (Vacuumbrand, PC 600). The reactor was loaded with the catalyst (0.5 g, particle size = 0.2–0.4 mm), diluted with quartz (0.5 g, particle size = 0.25–0.36 mm) and inserted in a tubular oven heated at 423 K. Thereafter, the pressure was set to 10 mbar and the liquid feed ( $0.1 \text{ cm}^3 \text{ min}^{-1}$ ) was admitted. Samples were periodically collected at the gas-liquid separator.

The concentration of reactants and products was determined by HPLC in a Merck LaChrom system equipped with a Biorad Aminex HPX-87H column heated at 308 K and a refractive index detector (Hitachi Chromaster model 5450) set at 303 K, using aqueous sulfuric acid (0.005 M,  $0.6 \text{ cm}^3 \text{ min}^{-1}$ ) as the eluent. Quantification was attained based on the absolute peak areas. Calibration curves were measured in the 0.1–10 wt.% range using glycerol and GC (Sigma-Aldrich, 90%). Glycerol 1,3-carbonate was not quantified since it was produced in trace amounts in all tests. The conversion of the substrate was calculated as the number of moles reacted divided by number of moles of the substrate fed and the yield of the product as the number of moles formed divided by the number of moles of glycerol fed, according to the following formulas, where the subscripts 0/1 refer to the reactor inlet/outlet mixture:

$$X_{\text{glycerol}} = 1 - (n_{\text{glycerol},1} / n_{\text{glycerol},0})$$

$$Y_{\text{GC}} = n_{\text{GC},1} / n_{\text{glycerol},0}$$

The carbon balance of continuous experiments was calculated as the ratio between the number of moles of products and the number of moles of glycerol fed and was always higher than 97%. The experimental error, determined by three repetitions of selected runs, was within 3%.

## Results and discussion

### Catalyst selection

In view of developing a catalyst suitable for the carbonation of glycerol with urea in continuous mode, one should consider the different conditions under which the material is utilised as compared to the so far investigated batch operation and their effect on the main catalyst descriptors, *i.e.*, activity, selectivity and stability. One key discrepancy is the requirement of a reaction medium, in view of the insufficient solubility of urea in glycerol at ambient temperature, which hinders the free flow of the neat reactants mixture. Thus, as a first step, several protic and aprotic polar liquids were tested to identify a suitable solvent. Amongst the protic media, water and short-chained alcohols enabled the complete dissolution of the triol and of urea, while alcohols with longer chains could only partially solubilise the reactants (Table 1). Aprotic liquids generally displayed a poorer dissolution ability, except for  $\gamma$ -butyrolactone (GBL) and dimethylsulfoxide (DMSO), which were found effective. Based on these findings, it was concluded that a high relative permittivity and the ability of forming strong hydrogen bonds are crucial features of a suitable medium.

To evaluate the degree of interaction of these polar solvents with the catalytic sites and the implications on the performance, batch tests were conducted with the most active

Table 1. Solvents screened for the dissolution of glycerol and urea and corresponding reaction rates obtained with ZnO.

Nature	Solvent	$\epsilon_r$	Dissolution	$Y_{\text{GC}}^d$ $\text{mmol h}^{-1} \text{g}^{-1}$
	None	-	-	68.6
Protic	Water	80.1	yes	1.1
	Methanol	32.6	yes	1.5
	Ethanol	24.3	yes	0.9
	2-Propanol	18.3	no	-
	1-Butanol	17.8	no	-
Aprotic	DMF <sup>a</sup>	36.7	no	-
	Ethyl acetate	6.0	no	-
	DMSO <sup>b</sup>	46.7	yes	6.6
	GBL <sup>c</sup>	41.8	yes	44.9
	Acetone	20.7	no	-
	Acetonitrile	35.9	no	-

<sup>a</sup> DMF = dimethylformamide; <sup>b</sup> DMSO = dimethyl sulfoxide; <sup>c</sup> GBL =  $\gamma$ -butyrolactone; <sup>d</sup> reaction conditions:  $T = 423 \text{ K}$ ,  $P = 10 \text{ mbar}$ ,  $t = 1 \text{ h}$ ,  $n_{\text{glycerol}}/n_{\text{urea}} = 1$ ,  $m_{\text{cat}}/m_{\text{glycerol}} = 0.1$ .

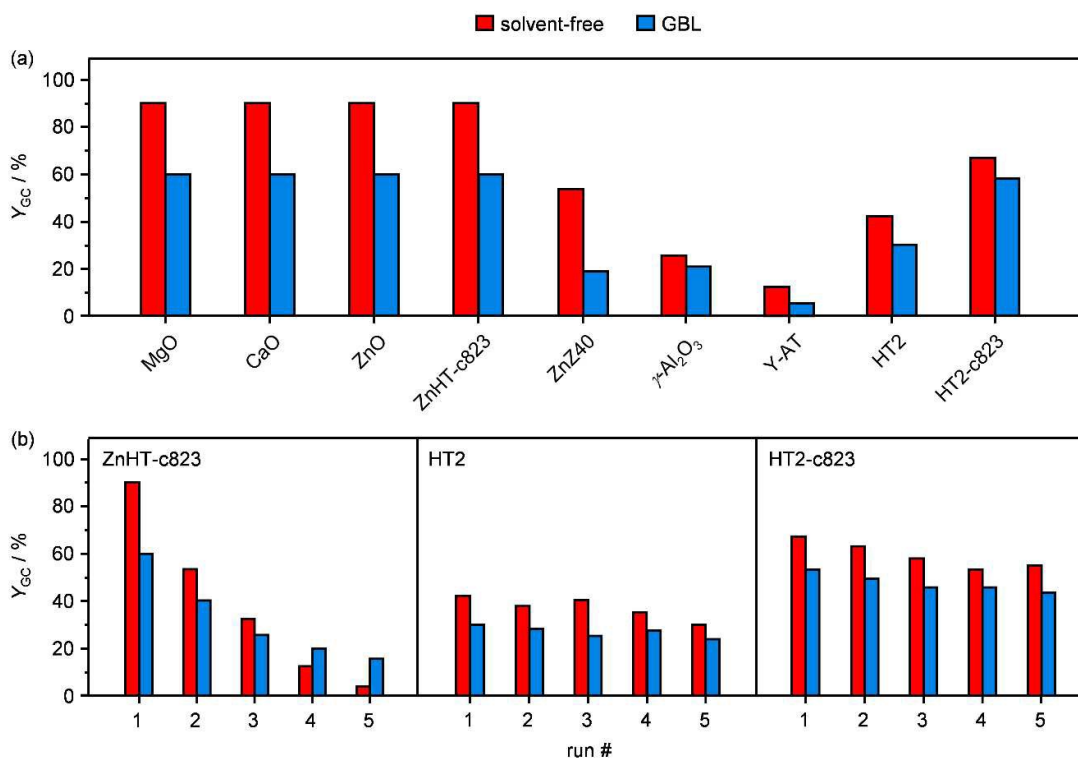


**Figure 2.** GC yield over (a) various catalysts and over (b) ZnHT-c823, Zn-Z40 and HT2-c823 in five consecutive reaction runs under solvent-free conditions (red) and in GBL (blue). Reaction conditions:  $T = 423$  K,  $P = 10$  mbar,  $t = 1$  h,  $n_{\text{glycerol}}/n_{\text{urea}} = 1$ ,  $m_{\text{cat}}/m_{\text{glycerol}} = 0.1$ .

material so far reported, *i.e.*, ZnO.<sup>[14]</sup> The use of any medium hindered the activity of the oxide (Table 1). A stronger depletion of the reaction rate was observed with the protic liquids. This was not surprising based on the proposed mechanism of glycerol activation on basic solids,<sup>[18]</sup> which comprises the deprotonation of a hydroxyl group. Protic solvents, especially those with a  $pK_a$  value comparable or lower with respect to that of glycerol, will compete with the triol for the active centres reducing the number of sites available for the desired transformation. In line with this reasoning, the aprotic DMSO and, especially, GBL reduced the reaction rates to a significantly lower extent. Based on this result and owing to its lower flammability, environmental hazard and higher biodegradability, the latter was considered for the subsequent studies. It should be noted that the presence of any solvent did not hinder the dissolution of ZnO. Aiming at identifying an effective active phase for the reaction, various solids that were assessed in batch mode under solvent-free conditions were evaluated in the presence of GBL in the same type of reactor (Figure 2a). Strongly basic oxides of widely available, cheap and non-toxic metals such as MgO and CaO displayed a high activity (70 and 64% GC yield, respectively), similarly to the case of ZnO. Materials in which zinc was introduced in a matrix, such as a Zn-Al mixed oxide (ZnHT-c823) prepared by calcination of a hydrotalcite ( $\text{Zn}_4\text{Al}_2(\text{OH})_{12}\text{CO}_3 \cdot x\text{H}_2\text{O}$ ) and a zeolite containing Zn cations at ion-exchange positions (ZnZ40) attained a GC yield of 60 and 18%, respectively. Based on previous reports indicating the beneficial effect of the co-presence of acidic and basic

functionalities for this transformation,<sup>[16a]</sup>  $\gamma$ -Al<sub>2</sub>O<sub>3</sub> and an alkaline-treated zeolite Y with a Si/Al ratio of 6 (Y-AT)<sup>[17]</sup> were also assessed. These solids were only very moderately active (24 and 6% GC yield, respectively). Finally, a Mg-Al hydrotalcite ( $\text{Mg}_4\text{Al}_2(\text{OH})_{12}\text{CO}_3 \cdot x\text{H}_2\text{O}$ , HT2) and the corresponding mixed oxide obtained by calcination (HT2-c823) showed a GC yield of 24 and 59%, in that order. The two best materials, the oxides of Mg and Ca, fully dissolved upon testing as ZnO (Figure S1), and were thus excluded from the subsequent investigations. The three best catalysts that did not appear to dissolve upon testing, *i.e.*, ZnHT-c823, HT2 and HT2-c823, were additionally evaluated in 5 reaction cycles performed at a conversion level lower than 100% to gather more insights into their stability. The former catalyst underwent a dramatic loss of activity ( $\sim 90\%$ , Figures 2b), which was rationalised based on the pronounced depletion of the original zinc content ( $\sim 65\%$  after the fifth reaction cycle). Oppositely, the decrease in GC yield was only within *ca.* 20% for both HT2 and HT2-c823 (Figure 2c,d) and the metals content was found unaltered after the repeated use. It is worth noting that over all materials the selectivity to GC was close to 100%, as the formation of by-products was negligible. These typically include glycerol 1,3-carbonate, which forms by addition of the terminal hydroxy-groups of the triol to urea, and glycidol, which is obtained by further conversion of glycerol 1,2-carbonate. The formation of the latter in trace amounts is in agreement with previous evidence,<sup>[16]</sup> and is expected to be even more hindered upon continuous operations, *i.e.* when the product is quickly removed from the catalytically active material.

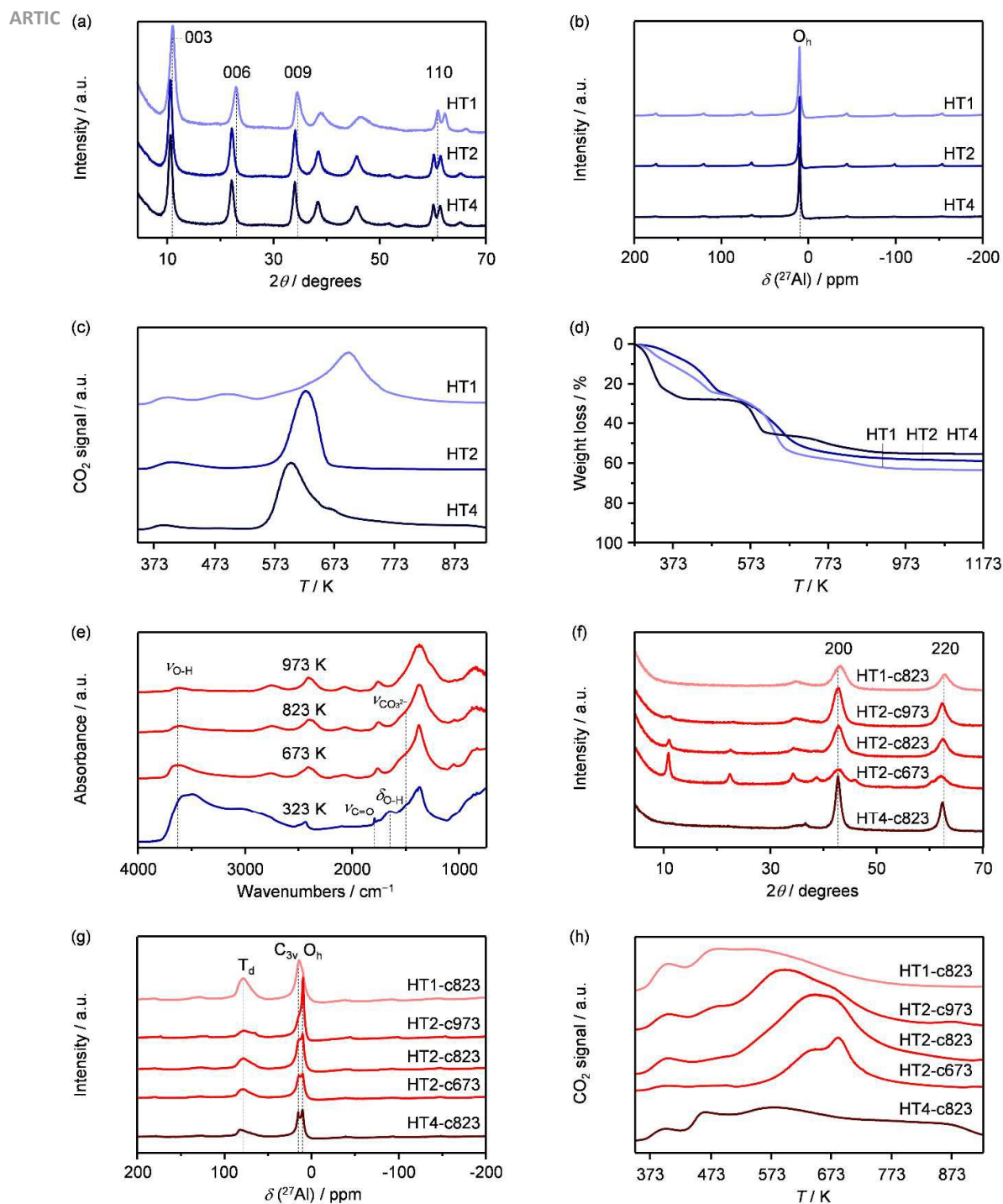


**Figure 3.** (a) XRD, (b)  $^{27}\text{Al}$  MAS NMR, (c)  $\text{CO}_2$ -TPD and (d) TGA profiles of the as-synthesised HTX materials; (e) DRIFT spectra of HT2 upon heating in inert gas; (f) XRD (g)  $^{27}\text{Al}$  MAS NMR and (h)  $\text{CO}_2$ -TPD profiles of the calcined HTX-c samples.

### Optimisation of Mg-Al-based materials

Since they demonstrated the best compromise between activity and stability and have an environmentally friendly composition, Mg-Al-containing solids were selected for further development. In order to improve their catalytic properties, efforts were made to establish structure–performance relations by modifying synthesis parameters. Specifically, additional hydrotalcite samples with nominal Mg/Al ratios of 1

and 4 were prepared and calcined at 823 K and the material with Mg/Al = 2 previously tested was alternatively activated at 673 or 973 K.

Concerning the as-coprecipitated materials, the metals content was found to be close to the targeted value in all cases and their surface area was *ca.*  $50\text{ m}^2\text{ g}^{-1}$ , in line with literature data (Table 2).<sup>[16b]</sup> The XRD patterns of these solids evidenced the typical reflections of a pure rhombohedral (3R) layered double hydroxide structure (Figure 3a).<sup>[19]</sup> As previously

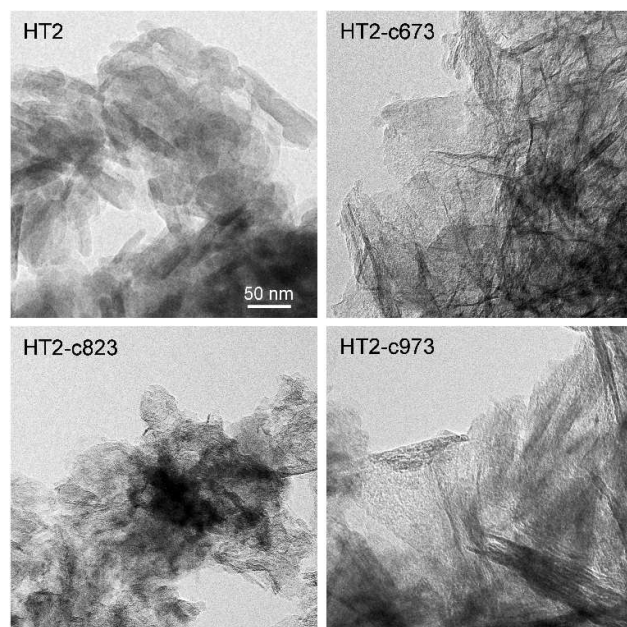


**Figure 4.** TEM images of the samples obtained upon the thermal decomposition of the HT2 precursor.

reported,<sup>[20]</sup> these reflections shifted to lower  $2\theta$  values for the materials with higher Mg/Al ratios owing to the expansion of the unit cell (Table 2). TEM imaging of HT2 confirmed the irregular plate-like morphology of the hydrothermal crystals, which exhibit extensive intergrowth and randomly oriented sheets (Figure 4). <sup>27</sup>Al MAS NMR spectra (Figure 3b) displayed a narrow signal centred at 10 ppm for all hydrothermalites, which supports the octahedral (O<sub>h</sub>) geometry of the Al species contained. The CO<sub>2</sub>-TPD (Figure 3c and Table 2) analysis revealed a small peak at ca. 400 K for all HTx samples, indicating the presence of a low amount of basic sites of mild nature. Based on a second weak signal at ca. 500 K, HT1 additionally possessed a fraction of moderately stronger sites. In all CO<sub>2</sub>-TPD curves, an intense and broad peak at  $T > 600$  K was evident, originated from the decomposition of interlayer carbonates leading to CO<sub>2</sub>. TGA (Figure 3d) evidenced a weight

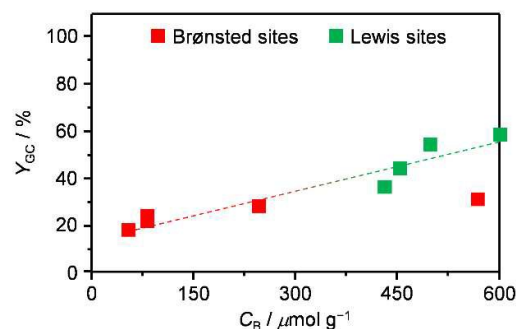


**Figure 5.** GC yield versus the concentration of basic sites for the as-prepared and calcined HTx catalysts. Reaction conditions:  $T = 423$  K,  $P = 10$  mbar,  $t = 1$  h,  $n_{\text{glycerol}}/n_{\text{urea}} = 1$ ,  $m_{\text{cat}}/m_{\text{glycerol}} = 0.1$ .

loss at ca. 400 K due to the desorption of water from the external surface and the interlayers for all materials. A second signal was observed at  $T > 600$  K, which descends from the decomposition of interlayer carbonates leading to CO<sub>2</sub>, as detected by CO<sub>2</sub>-TPD at the same temperature, and from the hydroxylation of the layers generating a mixed oxide and H<sub>2</sub>O. These modifications are further supported by DRIFT spectroscopy performed upon heating of HT2 in inert gas (Figure 3e). At 673 K, the broad band spanning from 3750 to 3000 cm<sup>-1</sup> due to the stretching of O-H bonds ( $\nu_{\text{O-H}}$ ) and that with maximum at 1640 cm<sup>-1</sup> related to the bending of O-H bonds ( $\delta_{\text{O-H}}$ ) present in the spectrum of HT2 were strongly depleted, in line with the loss of adsorbed water. At higher temperatures, the intensity of the residual  $\nu_{\text{O-H}}$  signal at ca. 3630 cm<sup>-1</sup> decreased and the decomposition of carbonate species completed leading to the disappearance of the absorption band at 1750 cm<sup>-1</sup> caused by the stretching of C=O bonds ( $\nu_{\text{C=O}}$ ) and of the shoulder at 1550 cm<sup>-1</sup> due to the asymmetric stretching of the bonds in the carbonate ion ( $\nu_{\text{CO}_3^{2-}}$ ). Upon calcination of the hydrothermalites at 823 K, a relatively disordered mixed metal oxide layered structure was formed, as indicated by broad XRD reflections at 43 and 62°  $2\theta$  (Figure 3f). The three samples were characterised by the same metals ratio as for the starting materials and by a surface area

**Table 2.** Characterisation and catalytic data of the hydrothermalites and the mixed metal oxides derived upon thermal activation.

Sample	Mg/Al <sup>a</sup>	Phase <sup>b</sup>	Unit cell size <sup>b</sup>		$S_{\text{BET}}^c$ m <sup>2</sup> g <sup>-1</sup>	$V_{\text{pore}}^d$ cm <sup>3</sup> g <sup>-1</sup>	$C_B^e$ μmol g <sup>-1</sup>	$T_{\text{des}}^f$ K	$T_{\text{dec}}^f$ K	$Y_{\text{GC}}^g$ %
			$a = b / \text{Å}$	$c / \text{Å}$						
HT1	1.27	HT	2.91	22.75	155	0.38	86	398	695	24
HT2	1.97	HT	3.00	22.82	88	0.47	58	495	599	17
HT4	3.52	HT	3.05	23.01	85	0.46	87	387	624	21
HT1-c823	1.10	MMO	-	-	207	0.59	434	401	-	31
HT2-c673	1.95	HT+MMO	-	-	224	0.62	439	538	681	38
HT2-c823	2.01	MMO	-	-	197	0.58	600	648	-	59
HT2-c973	1.97	MMO	-	-	210	0.87	501	641	-	56
HT4-c823	3.89	MMO	-	-	136	0.41	250	593	-	29
HT2-c823-r	1.94	HT	3.02	22.98	125	0.48	570	630	-	35

<sup>a</sup> XRF; <sup>b</sup> SRD; <sup>c</sup> BET method; <sup>d</sup> volume adsorbed at  $p/p_0 = 0.98$ ; <sup>e</sup> integrated area of CO<sub>2</sub>-TPD curves; <sup>f</sup> temperature corresponding to the maximum of the desorption (des) and decomposition (dec) peaks upon CO<sub>2</sub>-TPD analysis; <sup>g</sup> Reaction conditions:  $T = 423$  K,  $P = 10$  mbar,  $t = 1$  h,  $n_{\text{glycerol}}/n_{\text{urea}} = 1$ ,  $m_{\text{cat}}/m_{\text{glycerol}} = 0.1$ .

**Table 3.** Characterisation and catalytic data of the technical mixed metal-oxide catalysts studied.

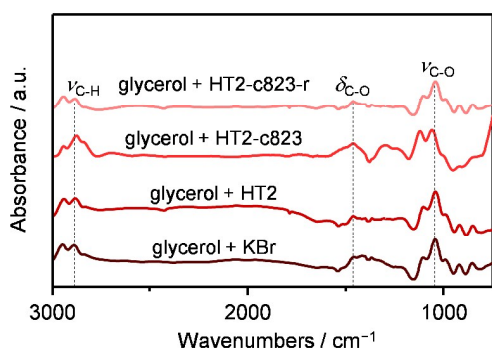
	Mg/Al <sup>a</sup>	S <sub>BET</sub> <sup>b</sup> m <sup>2</sup> g <sup>-1</sup>	V <sub>pore</sub> <sup>c</sup> cm <sup>3</sup> g <sup>-1</sup>	V <sub>macro</sub> <sup>d</sup> cm <sup>3</sup> g <sup>-1</sup>	V <sub>meso</sub> <sup>e</sup> cm <sup>3</sup> g <sup>-1</sup>	Crush strength N	C <sub>B</sub> <sup>f</sup> μmol g <sup>-1</sup>	ΔP <sup>g</sup> bar	Y <sub>GC</sub> <sup>h</sup> %
HT2-a-c823 <sup>i</sup>	1.06	101	0.59	0.17	0.31	<10	325	82	-
HT2-s-c823 <sup>i</sup>	2.11	130	0.61	0.19	0.40	<10	284	95	-
HT2-m-c823 <sup>i</sup>	2.56	90	0.38	0.17	0.20	16	290	42	-
HT2-k-c823 <sup>i</sup>	1.26	62	0.17	0.21	0.08	85	323	0	58
HT2-b-c823 <sup>i</sup>	1.85(1.83) <sup>j</sup>	83(48)	0.46(0.44)	0.24(0.21)	0.18(0.15)	90	383(326)	0	22

<sup>a</sup> XRF; <sup>b</sup> BET method; <sup>c</sup> volume adsorbed at P/P<sub>0</sub> = 0.98; <sup>d</sup> volume of Hg intruded into pores >50 nm in diameter; <sup>e</sup> volume of Hg intruded into pores of 3.7-50 nm diameter; <sup>f</sup> CO<sub>2</sub>-TPD; <sup>g</sup> pressure drop in the continuous reactor after 24 h; <sup>h</sup> reaction conditions: T = 423 K, P = 10 mbar, t = 1 h, n<sub>glycerol</sub>/n<sub>urea</sub> = 1, m<sub>cat</sub>/m<sub>glycerol</sub> = 0.1; <sup>i</sup> a = alumina, s = silica, m = montmorillonite, k = kaolin and b = bentonite; <sup>j</sup> values after use in the continuous reactor for 24 h in brackets.

of 140-210 m<sup>2</sup> g<sup>-1</sup>. TEM showed that the particle size and morphology was maintained after the thermal treatment (Figure 4) and confirmed the development of small intraparticle mesopores responsible for the surface area enhancement identified by N<sub>2</sub> sorption. Furthermore, comparison of the compositional uniformity by EDX spectroscopy evidenced a homogeneous distribution of the metals, with no visible phase separation after heating to 1023 K (Figure S2). In these materials, a part of the Al atoms acquired a tetrahedral geometry (T<sub>4</sub>), while the symmetry of a fraction of the remaining hexacoordinated centres changed to distorted octahedral (C<sub>3v</sub>), as indicated by the appearance of signals located at 80 and 18 ppm, respectively, and the decrease of the peak at 10 ppm in the <sup>27</sup>Al MAS NMR spectra (Figure 3g). The basicity of the calcined samples was higher than that of the precursors both in terms of number and strength of the sites (Figure 3h and Table 2) and strongly depended on the Mg/Al ratio. CO<sub>2</sub> desorbed from the solids with Mg/Al = 1 and 4 in a broad temperature range, indicating the coexistence of milder and stronger centres. For HT2-c823, the desorption peak showed a maximum at 650 K, hinting the dominance of stronger sites. Calcination of HT2 at 673 K led to an only partial decomposition of the hydroxalite to a mixed oxide. Indeed, the XRD pattern displayed peaks characteristic of both the double layered hydroxide and the Mg-Al oxide and the <sup>27</sup>Al MAS NMR spectrum indicated a greater retention of octahedral aluminium species (Figures 3f,g). The surface area increased by only 85% and the basicity of the material was intermediate between that of the non-calcined sample and

that of the one calcined at 823 K (Figure 3d and Table 2). When the heat treatment was performed at 973 K, the properties of the mixed oxide obtained were very similar to those of HT2-c823. The sample had a slightly higher crystallinity and, in line with this, an inferior surface area and basic strength. In agreement with the well-known memory effect of calcined hydroxalites,<sup>[18b]</sup> HT2-c823 almost fully recovered the double hydroxide structure upon rehydration. This is supported by the typical pattern of a hydroxalite observed in the XRD (Figure S3a) and by the minor part of Al atoms retaining a tetrahedral geometry detected by <sup>27</sup>Al MAS NMR (Figure S3b). This solid possessed an almost halved surface area (125 m<sup>2</sup> g<sup>-1</sup>) compared to the starting mixed oxide but a similar basicity. Accordingly, it is supposed that the higher strength of hydroxyl species compared to carbonates compensates for the lower available surface.

The catalytic performance of the newly prepared hydroxalites and mixed oxides was evaluated for the carbonation of glycerol with urea in batch mode under the same conditions applied to HT2 and HT2-c823. HT1 and HT4 attained a moderately higher GC yield compared to HT2, which further similarly increased upon calcination at 823 K for both samples (Table 2). Still, the latter values were only half of that exhibited by HT2 calcined at the same temperature. Thermal treatment of HT2 at 673 and 973 K led to inferior and comparable materials, respectively, with respect to HT2-c823. These findings point to the importance of the basicity for this reaction. Indeed, when the yield of GC is plotted against the amount of basic sites in the catalysts (Figure 5) a practically linear trend is observed. Interestingly, the data point corresponding to the rehydrated sample was an outlier, *i.e.*, it demonstrated a relatively poor yield in spite of its high basicity. Since CO<sub>2</sub>-TPD cannot differentiate between Lewis and Brønsted sites,<sup>[21]</sup> DRIFT spectroscopy (Figure 6) was applied as a tool to investigate the relevance of the basic character on the interaction between glycerol and the catalyst. The latter was very weak in the case of HT2, as the spectrum was virtually identical to that of condensed glycerol<sup>[22]</sup> and of glycerol in the presence of KBr. Conversely, when the reactant was contacted with HT2-c823, significant deviations were detected, including the blue-shift of the absorption frequency of the stretching of the C-O bond (ν<sub>C-O</sub>) from 1040 to 1055 cm<sup>-1</sup> and the red shift of that of the stretching of C-H bonds (ν<sub>C-H</sub>) from 2880 to 2874 cm<sup>-1</sup>. This, along with the appearance of a

**Figure 6.** DRIFT spectra of glycerol in the presence KBr, HT2, HT2-c823 and HT2-c823-r.

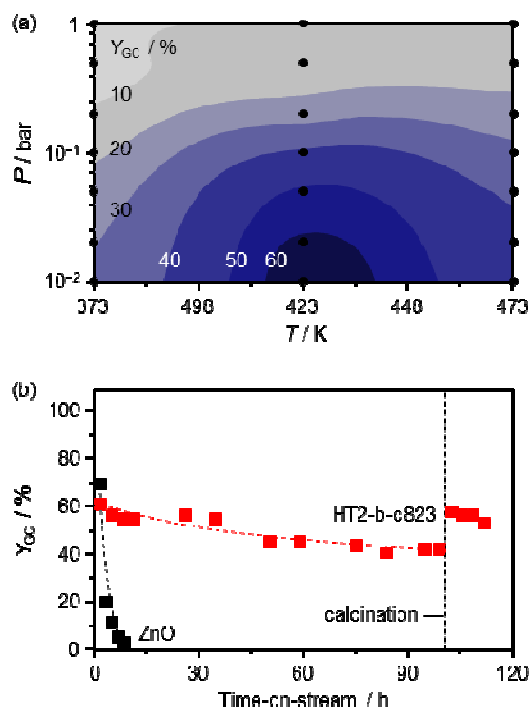


**Figure 7.** (a) GC yield versus reaction temperature and pressure; (b) evolution of the GC yield over 100 h and effect of regeneration by calcination of the used catalyst.

pronounced band centred at  $1451\text{ cm}^{-1}$  and overlapping with the one at  $1410\text{ cm}^{-1}$  typical of the bending mode of the C-O bond ( $\delta_{C-O}$ ) of pure glycerol,<sup>[22]</sup> suggest the formation of alkoxy species *via* dehydrogenation.<sup>[23]</sup> In the case of HT2-c823-r, the spectrum resembled that obtained in the experiment with HT2. Thus, considering the equivalent concentration and strength of basic sites in HT2-c823 and HT2-c823-r, the higher activity of the former is attributed to better capability of Lewis-basic sites to dehydrogenate glycerol as compared to Brønsted-basic centres.

#### Catalyst forming for the continuous manufacture of GC

Based on its superior performance, HT2-c823 was the most suited catalyst to demonstrate a continuous-flow technology. As a first step in this direction, the reaction temperature and pressure applied to the fixed-bed reactor were optimised by performing various measurements at a LHSV of  $12\text{ h}^{-1}$  for 1 h on stream (Figure 7a). The optimal value for the first parameter was found to be 423 K since, at lower and higher temperature, a diminished reaction kinetics and an increased formation of by-products (acetol, acrolein and oligomers), respectively, limited the GC yield. Regarding the pressure, sub-atmospheric conditions were beneficial, as observed for batch experiments.<sup>[14,16a]</sup> Catalytic tests conducted at 423 K and 10 mbar yielded 65% of the desired product, thus surpassing the batch results. This value is somewhat lower than what reported in the literature for basic materials.<sup>[12-15,16a]</sup> In this respect, it should be noted that in this work a unitary urea/glycerol ratio was used, while those studies applied a ratio of 2, which leads to kinetic advantages. In spite of its high activity, when the catalyst was tested for a longer time on

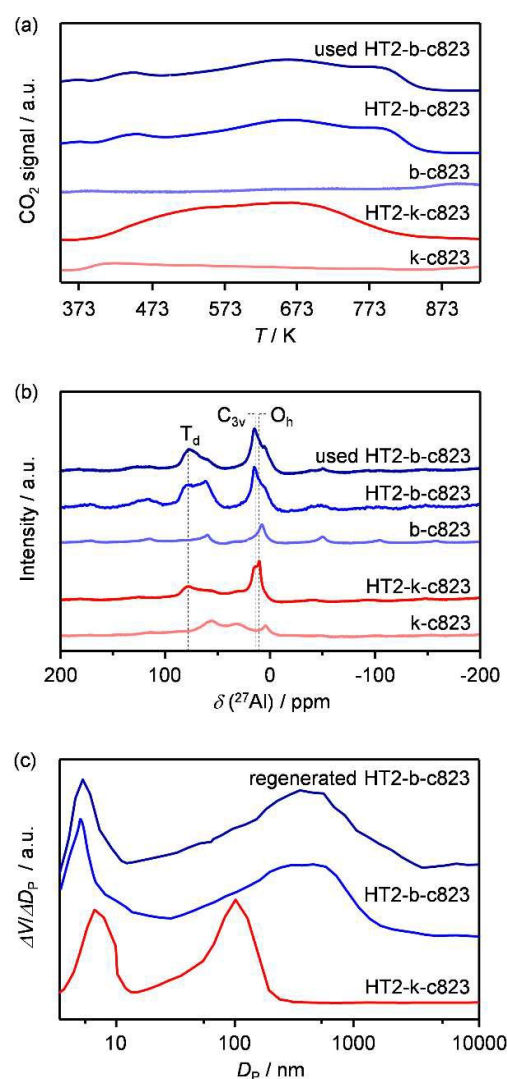


**Figure 8.** (a) CO<sub>2</sub>-TPD and (b) <sup>27</sup>Al MAS NMR of the materials shaped with bentonite and kaolin, the respective binders and HT2-b-c823 after use. (c) Pore size distribution of HT2-k-c823 and HT2-b-c823 in its fresh and calcined forms.

stream, a very fast activity loss was observed (Figure S4). This was explained based on the poor mechanical stability of the 0.2-0.4 mm particles obtained by crushing of catalyst pellets (Table 3), which caused an increase of the system pressure (Figure S4) and, thus, hindered the removal of ammonia.

In practise, such operational issues are typically avoided by shaping the active phase with a binder into mechanically-stable, millimetre-sized catalyst bodies.<sup>[2]</sup> Despite the relevance, the formulation of technical catalysts, which requires the harmonisation of multiple interacting component phases during the preparation and application, lacks fundamental guidelines. To approach this, the development of a technical material by the common shaping method of extrusion was tackled. The protocol involved mixing the dry components with water, extrusion of the resulting paste into cylindrical bodies of 2 mm in diameter and drying and hardening by calcination at high temperature the resulting bodies to ensure a strong interaction between the active

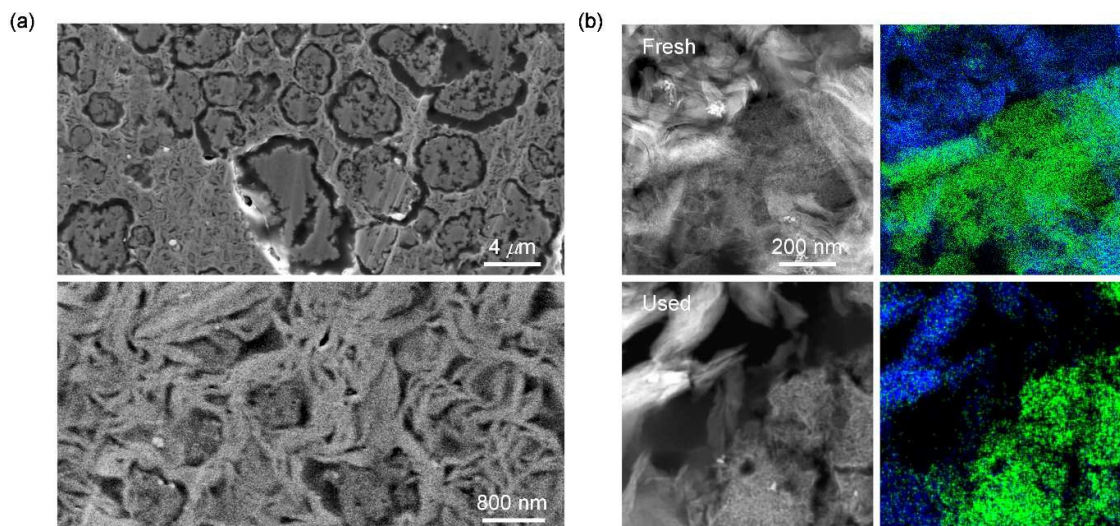


**Figure 9.** (a) SEM images of an ion beam-etched section of HT2-b-c823; (b) HAADF images and corresponding elemental maps of magnesium (green) and silicon (blue) of cross-sectional areas of the technical catalyst prepared with bentonite in fresh and used forms. The corresponding EDX spectra are reported in Figure S5.

phase and binder particles. Since the temperature of hardening is similar to that applied during the thermal activation of the hydrotalcite, it was decided to shape the precursor rather than the mixed metal oxide, thus reducing the energy requirements of the synthesis by avoiding a calcination step. Materials commonly applied to enhance the mechanical strength of technical catalysts include silicas, aluminas and natural clays, which are typified by their low cost and wide availability. Despite the general preconception that a binder should be inert, there is growing awareness that these phases can impact the catalytic performance with both beneficial and detrimental consequences. This could result from several reasons including the presence of additional active sites in the binder and/or the modification of the nature or accessibility of active sites in the active phase. Moreover, the particle properties of the binder determine the organisation and related interparticle pore architecture controlling mass transport in the technical shape.

To screen the potential compatibility, five representative binders (silica, alumina, bentonite, montmorillonite and kaolin) were tested in their pure calcined forms (Table S2). As expected, none of the materials demonstrates significant activity, in agreement with the negligible concentrations of basic sites evidenced by CO<sub>2</sub>-TPD. Upon testing the technical catalysts obtained upon extrusion with the hydrotalcite, alumina, silica and montmorillonite did not provide the desired mechanical stability (Table 3). Comparatively, bentonite and kaolin led to a high side crush strength, and no pressure drop developed over the resulting bodies over a 24 h run. Nevertheless, while the bentonite-containing solid displayed an initial GC yield similar to the powder catalyst (Table 3), only a third of the desired product formed over HT2-k-c823. To explain the different performance, the porosity, structure and basic properties of the kaolin- and bentonite-containing samples were characterised in depth. Analysis by CO<sub>2</sub>-TPD revealed subtle differences in the comparative amount and strength of basic sites (Figure 8a), evidencing a higher fraction

of strong basic sites (centred at 790 K) in the bentonite-containing solid with respect to the catalyst extruded with kaolin. The basic sites distribution differed noticeably with respect to the dominant peak observed at 650 K in the pure Mg-Al mixed oxide (Figure 3h). Since the calcined bentonite exhibited no basic sites, it was deduced that the interaction between the hydrotalcite and the binder during shaping influenced the nature of the sites generated upon thermal activation. This is supported by the fact that the <sup>27</sup>Al MAS NMR spectrum of HT2-b-c823 is not simply a linear combination of the aluminium species of the component phases, exhibiting a more complex line shape associated with tetrahedral aluminium (Figure 8b). Apart from possessing stronger basic sites, the bentonite-containing extrudate also displayed enhanced (meso- and macro-) porosity with respect to the kaolin-bound analogue (Figure 8c), which suggests an improved active site accessibility in the former sample. To confirm the structural uniformity, the spatial organisation of the active phase and the binder in HT2-b-c823 was analysed at different length scales. In particular, ion-beam-etched cross-sections of the extrudates by SEM confirmed that the active phase was well dispersed within the binder (Figure 9a). Higher-resolution analysis of microtome-cut cross-sections by STEM-EDX corroborated the intimate mixture of mixed oxide and binder particles, clearly revealing the extensive mesoporosity of the former (Figure 9b).

A 100-h catalytic test was performed to evaluate the long-term performance of the HT2-b-c823 catalyst (Figure 7b). The GC yield remained at the initial value of ca. 60% for about one third of the time-on-stream and only slightly (< -20%) decreased thereafter. This is in striking contrast with the behaviour of ZnO, which fully loses its activity within 6 h due to complete dissolution. In order to assess whether the alteration of the catalyst was reversible, analyses were conducted to unravel which of the four main mechanisms of deactivation typical of the liquid-phase conversion of bio-based feedstocks<sup>[24]</sup> were relevant. They comprise leaching of one or

more metals, amorphisation, restructuring of the basic sites and fouling. The first phenomenon was ruled out by elemental characterisation (Table 3), which demonstrated no alteration in the Mg and Al ratio. Nevertheless, both the surface area and the basicity of the catalyst decreased by ca. 40% after use (Table 3). This was attributed to the deposition of carbonaceous species on the surface rather than to a modification of the structure of the active phase. Indeed, TGA indicated a weight loss of around 20% at 673 K (Figure S6) and the porous and basic properties of HT2-b-c823 (Figure 8c) were recovered after calcination at 823 K for 5 h, while the structural and compositional organisation was preserved (Figure 9b). In line with this, a fully restored catalytic activity was observed at the beginning of a second catalytic run (Figure 7b). The remarkable stability and selectivity of the heterogeneous catalyst are key towards a sustainable continuous glycerol carbonate manufacture. Indeed, they lower the energy required for its regeneration and simplify the isolation of the product from the outlet stream. It should be noted that the incomplete glycerol conversion is likely to have a limited impact on the ecologic and economic footprint of the process, since the triol can be easily separated from the carbonate by distillation owing to its much higher boiling point.

## Conclusions

This study describes the design of a green heterogeneous catalyst in technical form which enables for the first time a continuous process to produce glycerol carbonate from glycerol and urea. Mixed oxides of the widely available and cheap Mg and Al metals obtained by thermal activation of hydrotalcites were identified as suitable catalysts for this transformation, displaying a remarkable activity and a much higher stability in repeated reaction cycles than the state-of-the-art Zn-containing oxides, owing to their outstanding resistance against leaching. Additionally, their performance was only moderately affected by the presence of the polar yet aprotic  $\gamma$ -butyrolactone as solvent, which is required in view of a continuous operation due to the poor solubility of urea in glycerol. Upon tuning of the composition and calcination temperature of the parent material, a glycerol carbonate yield as high as 60% was achieved in batch testing. In-depth characterisation indicated that the activity arises from the strong Lewis basicity of the material, which was demonstrated more effective in the activation of the substrate by deprotonation with respect to Brønsted-type basicity. Operation in continuous mode was shown to be feasible after identification of the optimal reaction conditions and the development of a protocol to produce an effective technical catalyst. Concerning the first issue, it was found essential to operate the reactor at sub-atmospheric pressure. With respect to the second aspect, it was uncovered that mixing the hydrotalcite with water and the natural and abundant clay bentonite as binder, followed by extrusion, drying and calcination enabled the preparation of a mechanically stable material possessing desirable basic properties and a well-

developed porosity at the meso and macro levels, and thus showing the same performance as the best mixed oxide in powder form. Upon a 100-h run, only moderate deactivation by fouling was observed and burning-off of the carbonaceous deposits was effective in fully recovering the catalyst functionality. Accordingly, this catalytic system holds the potential to be a more sustainable technology for the valorisation of the waste feedstock into a relevant chemical than that currently applied, which is based on homogeneous salts of heavy metals.

## Acknowledgements

This work was supported by the Swiss National Science Foundation (Project Number 200020-159760). Dr. A. J. Martín is acknowledged for the SEM analysis.

## References

- (a) G. W. Huber, S. Iborra and A. Corma, *Chem. Rev.*, 2006, **106**, 4044-4098; (b) J. N. Chheda, G. W. Huber and J. A. Dumesic, *Angew. Chem. Int. Ed.*, 2007, **46**, 7164-7183; (c) R. O. M. A. de Souza, L. S. M. Miranda and R. Luque, *Green Chem.*, 2014, **16**, 2386-2405.
- (a) S. Mitchell, N.-L. Michels and J. Pérez-Ramírez, *Chem. Soc. Rev.*, 2013, **42**, 6094-6112; (b) J. S. J. Hargreaves and A. L. Munnoch, *Catal. Sci. Technol.*, 2013, **3**, 1165-1171.
- (a) J.-P. Lange and C. M. A. M. Mesters, *Appl. Catal., A*, 2001, **210**, 247-255; (b) A. Corma, M. Grande, V. Fornés, S. Cartledge and M. P. Shatlock, *Appl. Catal.*, 1990, **66**, 45-57.
- (a) M. Morales, P. Y. Dapsens, I. Giovinazzo, J. Witte, C. Mondelli, S. Papadokonstantakis, K. Hungerbühler and J. Pérez-Ramírez, *Energy Environ. Sci.*, 2015, **8**, 558-567; (b) G. M. Lari, C. Mondelli, S. Papadokonstantakis, M. Morales, K. Hungerbühler and J. Pérez-Ramírez, *React. Chem. Eng.*, 2016, **1**, 106-118.
- (a) B. Schöffner, F. Schöffner, S. P. Verevkin and A. Börner, *Chem. Rev.*, 2010, **110**, 4554-4581; (b) K. Ueno and H. Mizushima, *US Pat.*, 0213517, 2007; (c) A. T. Brooker, *EP Pat.*, 2380958, 2011.
- (a) M. Ghandi, A. Mostashari, M. Karegar and M. Barzegar, *J. Am. Oil Chem. Soc.*, 2007, **84**, 681-685; (b) J. C. Fang, *US Pat.*, 2967173, 1961; (c) K. İlayç, S. Dumarçay, E. Fredon, C. Gérardin, A. Lemor and P. Gérardin, *J. Appl. Polym. Sci.*, 2011, **120**, 2354-2360.
- (a) J. Hu, J. Li, Y. Gu, Z. Guan, W. Mo, Y. Ni, T. Li and G. Li, *Appl. Catal., A*, 2010, **386**, 188-193; (b) S. Franklin, *US Pat.*, 2446145, 1948; (c) C. Vieville, J. W. Yoo, S. Pelet and Z. Mouloungui, *Catal. Lett.*, 1998, **56**, 245-247.
- M. Aresta, A. Dibenedetto, F. Nocito and C. Ferragina, *J. Catal.*, 2009, **268**, 106-114.
- C. Hammond, J. A. Lopez-Sanchez, M. Hasbi Ab Rahim, N. Dimitratos, R. L. Jenkins, A. F. Carley, Q. He, C. J. Kiely, D. W. Knight and G. J. Hutchings, *Dalton Trans.*, 2011, **40**, 3927-3937.
- (a) M. O. Sonnat, S. Amigoni, E. P. Taffin de Givenchy, T. Darmanin, O. Choulet and F. Guittard, *Green Chem.*, 2013, **15**, 283-306; (b) S. Claude, Z. Mouloungui and J. Yoo, *US Pat.*, 6025504, 2000.
- P. Barbaro and F. Liguori, *Chem. Rev.*, 2009, **109**, 515-529.
- L. Wang, Y. Ma, Y. Wang, S. Liu and Y. Deng, *Catal. Commun.*, 2011, **12**, 1458-1462.
- H. Hattori, *Appl. Catal., A*, 2001, **222**, 247-259.

## ARTICLE

## Journal of Materials Chemistry A

- 14 S. Fujita, Y. Yamanishi and M. Arai, *J. Catal.*, 2013, **297**, 137-141.
- 15 Q. Li, W. Zhang, N. Zhao, W. Wei and Y. Sun, *Catal. Today*, 2006, **115**, 111-116.
- 16 (a) M. J. Climent, A. Corma, P. De Frutos, S. Iborra, M. Noy, A. Velty and P. Concepción, *J. Catal.*, 2010, **269**, 140-149; (b) S. Abelló, F. Medina, D. Tichit, J. Pérez-Ramírez, J. C. Groen, J. E. Sueiras, P. Salagre and Y. Cesteros, *Chem. Eur. J.*, 2005, **11**, 728-739.
- 17 G. M. Lari, B. Puértolas, M. S. Frei, C. Mondelli and J. Pérez-Ramírez, *ChemCatChem*, 2016, **8**, 1507-1514.
- 18 B. Katryniok, S. Paul and F. Dumeignil, *ACS Catal.*, 2013, **3**, 1819-1834.
- 19 F. Cavani, F. Trifirò and A. Vaccari, *Catal. Today*, 1991, **11**, 173-301.
- 20 D. G. Cantrell, L. J. Gillie, A. F. Lee and K. Wilson, *Appl. Catal., A*, 2005, **287**, 283-190.
- 21 Q. Wang, J. Luo, Z. Zhong and A. Borgna, *Energy Environ. Sci.*, 2011, **4**, 42-55.
- 22 V. P. Indran, N. A. S. Zuhaimi, M. A. Deraman, G. P. Maniam, M. M. Yusoff, T.-Y. Y. Hin and M. H. A. Rahim, *RSC Adv.*, 2014, **4**, 25257-25267.
- 23 G. M. Lari, K. Desai, C. Mondelli and J. Pérez-Ramírez, *Catal. Sci. Technol.*, 2016, **6**, 2706-2714.
- 24 G. M. Lari, P. Y. Dapsens, D. Scholz, S. Mitchell, C. Mondelli and J. Pérez-Ramírez, *Green Chem.*, 2016, **18**, 1249-1260.